A New Parameterization of the Accretion of Cloud Water by Graupel and Its Evaluation through Cloud and Precipitation Simulations

HAN-GYUL JIN

School of Earth and Environmental Sciences, Seoul National University, Seoul, South Korea

HYUNHO LEE

School of Earth and Environmental Sciences, Seoul National University, Seoul, South Korea, and Center for Climate Systems Research, Columbia University, New York, New York

JONG-JIN BAIK

School of Earth and Environmental Sciences, Seoul National University, Seoul, South Korea

(Manuscript received 17 August 2018, in final form 20 November 2018)

ABSTRACT

A new parameterization of the accretion of cloud water by graupel for use in bulk microphysics schemes is derived by analytically integrating the stochastic collection equation (SCE). In this parameterization, the collection efficiency between graupel particles and cloud droplets is expressed in a functional form using the data obtained from a particle trajectory model by a previous study. The new accretion parameterization is evaluated through box model simulations in comparison with a bin-based direct SCE solver and two previously developed accretion parameterizations that employ the continuous collection equation and a simplified SCE, respectively. Changes in cloud water and graupel mass contents via the accretion process predicted by the new parameterization are closest to those predicted by the direct SCE solver. Furthermore, the new parameterization predicts a decrease in the cloud droplet number concentration that is smaller than the decreases predicted by the other accretion parameterizations, consistent with the direct SCE solver. The new and the other accretion parameterizations are implemented into a cloud-resolving model. Idealized deep convective cloud simulations show that among the accretion parameterizations, the new parameterization predicts the largest rate of accretion by graupel and the smallest rate of accretion by snow, which overall enhances rainfall through the largest rate of melting of graupel. Real-case simulations for a precipitation event over the southern Korean Peninsula show that among the examined accretion parameterizations, the new parameterization simulates precipitation closest to observations. Compared to the other accretion parameterizations, the new parameterization decreases the fractions of light and moderate precipitation amounts and increases the fraction of heavy precipitation amount.

1. Introduction

For several decades, cloud-resolving models have been developed to simulate clouds and precipitation with greater realism and to understand cloud-related processes better. Cloud microphysics schemes, which represent formation, growth, and sedimentation processes of hydrometeor particles, are a crucial element of cloud-resolving models. Various cloud microphysics schemes that include different assumptions and have different degrees of complexity have been proposed.

Two types of cloud microphysics schemes are widely used: bin microphysics schemes and bulk microphysics schemes. Bin microphysics schemes (e.g., Stevens et al. 1996; Lynn et al. 2005; Khain et al. 2011) predict the number concentration of each hydrometeor in each size bin and hence the temporal evolution of size distributions of hydrometeor particles. However, they require a great amount of computational resources, inhibiting their operational use in precipitation prediction. Bulk microphysics schemes (e.g., Morrison et al. 2005; Milbrandt and Yau 2005; Hong and Lim 2006; Thompson et al. 2008; Mansell and Ziegler 2010) are relatively efficient because the size distributions of hydrometeor particles

Corresponding author: Jong-Jin Baik, jjbaik@snu.ac.kr

DOI: 10.1175/JAS-D-18-0245.1

are specified so that only a few prognostic variables for hydrometeors are predicted. As a result, diverse bulk microphysics schemes are being used for operational precipitation prediction.

In many bulk microphysics schemes, rimed ice hydrometeor species that have greater density and terminal velocity compared to snow are categorized as graupel or sometimes hail. In the cloud-resolving model simulations, graupel-related microphysical processes have great impacts on the amount and spatial distribution of surface precipitation when melting of graupel is a major source of rain in convective storms (Lin et al. 2005; Wang and Georgakakos 2005).

The collection process, which refers to the growth of hydrometeor particles through collision–coalescence, can be expressed by the stochastic collection equation (SCE); this equation is also called the kinetic collection equation, population balance equation, or Smoluchowski equation. However, many bulk microphysics schemes still parameterize the accretion of cloud water by graupel using the simple continuous collection equation. Several attempts have been made to derive an analytic solution of the SCE for the accretion of cloud water by graupel (Verlinde et al. 1990; Gaudet and Schmidt 2005; Seifert and Beheng 2006). Some bulk microphysics schemes employ simplified analytic solutions of the SCE obtained under some assumptions (Gaudet and Schmidt 2005; Seifert and Beheng 2006). In contrast to bulk microphysics schemes, bin microphysics schemes calculate the collection process by explicitly solving the SCE, which requires a much greater amount of computational resources.

The complexity of the exact solution is mainly attributed to the absolute value of the velocity difference between two colliding hydrometeor particles in the collection kernel used in the SCE (Gaudet and Schmidt 2005). Wisner et al. (1972) obtained a simplified solution by replacing the velocity difference by the difference in mass-weighted velocities; this approximation is generally called the Wisner approximation. Because some major disadvantages of the conventional Wisner approximation have been reported, it has been modified into different forms in several studies (Murakami 1990; Mizuno 1990; Gaudet and Schmidt 2005; Seifert and Beheng 2006). Gaudet and Schmidt (2005) approximated the absolute value of the velocity difference as the velocity difference itself and obtained a solution that consists of six terms involving gamma functions. Based on Gaudet and Schmidt (2005), Kovačević and Ćurić (2013) obtained a solution considering lower and upper limits of size of colliding particles other than zero and infinity, respectively. Verlinde et al. (1990) solved the SCE for the collection between two hydrometeor species using power laws to describe their masses and terminal velocities as a function of radius and gamma distributions to describe their size distributions. However, the solution includes general hypergeometric functions, so it is too computationally expensive to be used in numerical models.

In solving the SCE, the collection efficiency is commonly assumed to be a constant or a function based on the mean sizes of colliding hydrometeor species. Lee and Baik (2017) employed the collection efficiency that is expressed as a function of the sizes of the individual colliding particle pair and obtained an analytic solution of SCE to parameterize the autoconversion process of cloud water. Compared to the previous solutions of the autoconversion process, the solution of Lee and Baik (2017) is more complicated but calculates changes in the mass content and number concentration of cloud droplets more accurately. This implies that a more elaborate accretion parameterization can also be developed by employing the particle size–dependent collection efficiency, which motivates the present study.

In this study, the accretion of cloud water by graupel is parameterized based on an analytic solution of the SCE. The particle size–dependent collection efficiency that is obtained from a particle trajectory model by Khain et al. (2001) is used for the parameterization. In section 2, the bulk accretion parameterizations used in previous studies are summarized. In section 3, the derivation of a new accretion parameterization is given. In section 4, the new parameterization is evaluated through box model simulations. In section 5, the new parameterization is evaluated through cloud-resolving model simulations that include real-case simulations as well as idealized simulations. A summary and conclusions are presented in section 6.

2. Review of previous accretion parameterizations

Many bulk cloud microphysics schemes have employed the continuous collection equation to parameterize accretion processes (Morrison et al. 2005; Hong and Lim 2006; Thompson et al. 2008). In the parameterizations, it is assumed that the radii of cloud droplets in the collision cross section of the collection kernel and the terminal velocities of cloud droplets are negligible compared to those of large particles and that the collection efficiency between large particles and cloud droplets is constant. Wisner et al. (1972) parameterized the accretion of cloud water by hail with this method. Many bulk microphysics schemes have applied the method in the accretion of cloud water by graupel:

$$\left.\frac{\partial L_g}{\partial t}\right|_{\text{acc}} = \int_0^\infty L_c \pi R^2 v_{t,g}(R) \eta f_g(R)\, dR, \tag{1}$$

where L_g and L_c are the mass contents of graupel and cloud water, respectively; R is the radius of a graupel particle; $v_{t,g}$ is the terminal velocity of the graupel particle; η is the collection efficiency between graupel particles and cloud droplets; and $f_g(R)dR$ is the number concentration of graupel particles in the size interval $[R, R + dR]$. The subscript "acc" refers to the accretion process.

Owing to the simplicity of this method, which was introduced by Wisner et al. (1972), it has been included in many bulk microphysics schemes with various forms of terminal velocities and size distributions of graupel particles. For example, Thompson et al. (2008) integrated (1) assuming a power-law terminal velocity and a gamma size distribution for graupel particles. If the shape parameter of the gamma size distribution for graupel particles is set to 0, which is the default value in the Thompson microphysics scheme in the Weather Research and Forecasting (WRF) Model, the following parameterization is obtained:

$$\left.\frac{\partial L_g}{\partial t}\right|_{\text{acc}} = L_c \pi \left(\frac{\rho_0}{\rho}\right)^{1/2} v_{0,g} \overline{\eta} N_{0,g} \frac{\Gamma(3+\gamma_g)}{\lambda_g^{3+\gamma_g}}, \tag{2}$$

where ρ is the air density; ρ_0 is the reference air density; $v_{0,g}$ and γ_g are the velocity power-law constants; $N_{0,g}$ and λ_g are the intercept and slope parameters of the graupel size distribution, respectively; and Γ is the gamma function. The accretion parameterization, (2), is called W72 hereafter. The density factor $(\rho_0/\rho)^{1/2}$ represents the increase in the terminal velocities of particles with the decrease in air density. The bulk collection efficiency $\overline{\eta}$ is determined by the median volume diameter of cloud droplets and the mass-weighted mean diameter of graupel particles, following Cober and List (1993).

In most situations, the assumption of negligible sizes and terminal velocities of cloud droplets in W72 may be reasonable. However, when graupel particles are small in size, the sizes and terminal velocities of cloud droplets can change the swept volume significantly, making the assumption unrealistic.

Milbrandt and Yau (2005) used the SCE to parameterize the accretion process. By neglecting the terminal velocities of cloud droplets and adopting the bulk collection efficiency obtained by Cober and List (1993), the accretion process is parameterized as follows:

$$\left.\frac{\partial L_g}{\partial t}\right|_{\text{acc}} = \frac{4}{3}\pi^2 \rho_w \left(\frac{\rho_0}{\rho}\right)^{1/2} v_{0,g} \overline{\eta} N_{0,g} N_{0,c} \times \left[\frac{\Gamma(3+\gamma_g)\Gamma(\mu_c+4)}{\lambda_g^{3+\gamma_g}\lambda_c^{\mu_c+4}} + \frac{2\Gamma(2+\gamma_g)\Gamma(\mu_c+5)}{\lambda_g^{2+\gamma_g}\lambda_c^{\mu_c+5}} + \frac{\Gamma(1+\gamma_g)\Gamma(\mu_c+6)}{\lambda_g^{1+\gamma_g}\lambda_c^{\mu_c+6}}\right], \tag{3}$$

where ρ_w is the liquid water density and $N_{0,c}$, λ_c, and μ_c are the intercept, slope, and shape parameters of the gamma size distribution of cloud droplets, respectively. The accretion parameterization, (3), is called MY05 hereafter. Unlike W72, MY05 does not assume negligible sizes of cloud droplets when considering the swept volume. Among the three terms on the right-hand side of (3), the first term is exactly the same as (2), and the second and third terms correspond to the difference between W72 and MY05.

3. Derivation of a new accretion parameterization

The derivation of a new parameterization of the accretion process begins with the well-known SCE, which describes the rate of change in the particle number concentration induced by the collection process:

$$\frac{\partial f_g(m)}{\partial t} = \int_0^m f_g(m-m')K(m-m',m')f_c(m')\,dm' - \int_0^\infty f_g(m)K(m,m')f_c(m')\,dm', \tag{4}$$

where $f_g(m)dm$ and $f_c(m)dm$ are the number concentrations of graupel particles and cloud droplets in the mass interval $[m, m + dm]$, respectively, and K is the collection kernel. The right-hand side of (4) consists of two terms. The first term is a source term for graupel particles of mass m due to the collection of cloud droplets of mass m' by graupel particles of mass $m - m'$, and the second term is a sink term for graupel particles of mass m due to the collection of cloud droplets of mass m' by graupel particles of mass m. Note that the upper limit of the first term is m, because this term represents the collisions between two different types of hydrometeors. The collection kernel K is expressed as the product of the geometric swept volume per unit time and the collection efficiency:

$$K(r,r') = \pi(r+r')^2 |v_{t,g}(r) - v_{t,c}(r')|\eta, \tag{5}$$

where r and r' are the radii of graupel particles and cloud droplets, respectively; $v_{t,g}(r)$ and $v_{t,c}(r')$ are the terminal velocities of graupel particles and cloud droplets, respectively; and η is the collection efficiency. The collection efficiency is the product of the collision efficiency

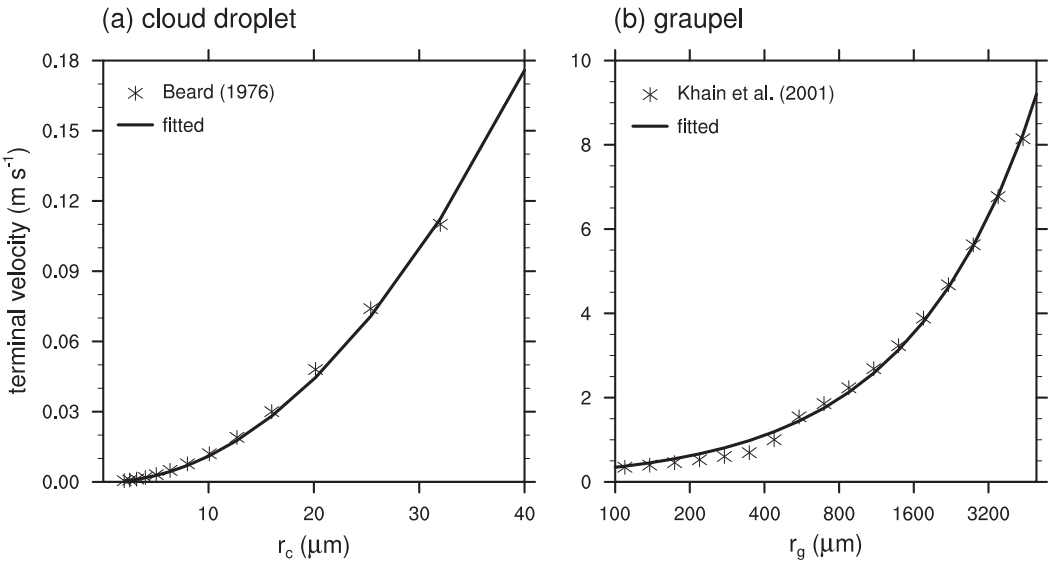

FIG. 1. Terminal velocities of (a) cloud droplets from Beard (1976) and (b) graupel particles from Khain et al. (2001) and the fitted function.

and the coalescence efficiency. The coalescence efficiency is assumed to be unity, which means that all accreted cloud droplets freeze on the graupel particles. Hence, the collection efficiency is equal to the collision efficiency.

By integrating (4) for all masses of graupel particles, the accretion rate can be obtained as

$$\left.\frac{\partial L_g}{\partial t}\right|_{\text{acc}} = \int_0^\infty \int_0^m m f_g(m-m') K(m-m', m') f_c(m')\, dm'\, dm - \int_0^\infty \int_0^\infty m f_g(m) K(m, m') f_c(m')\, dm'\, dm\,. \quad (6)$$

By substituting the variables in the first term on the right-hand side of (6) ($m - m' \to M$, $m' \to m$) and the second term ($m \to M$, $m' \to m$), (6) is reduced to a simpler form:

$$\left.\frac{\partial L_g}{\partial t}\right|_{\text{acc}} = \int_0^\infty \int_0^\infty m f_g(M) K(M, m) f_c(m)\, dm\, dM\,. \quad (7)$$

Using radius quantities instead of mass quantities, (7) is rewritten as

$$\left.\frac{\partial L_g}{\partial t}\right|_{\text{acc}} = \frac{4}{3}\pi\rho_w \int_0^\infty \int_0^\infty r^3 f_g(R) K(R, r) f_c(r)\, dr\, dR\,. \quad (8)$$

The size distribution function of graupel particles $f_g(R)$ is expressed by an exponential function, and the size distribution function of cloud droplets $f_c(r)$ is expressed by a gamma distribution:

$$f_g(R) = N_{0,g} \exp(-\lambda_g R), \quad (9a)$$

$$f_c(r) = N_{0,c} r^{\mu_c} \exp(-\lambda_c r), \quad (9b)$$

where $N_{0,g}$ and $N_{0,c}$ are the intercept parameters, μ_c is the shape parameter, and λ_g and λ_c are the slope parameters. Each distribution has been assessed as describing the observed size distributions of each hydrometeor well (Pruppacher and Klett 1997). Following the method used in Thompson et al. (2008), the shape parameter is diagnosed empirically as $\mu_c = \min[15, \text{nint}(10^9/N_c + 2)]$, where N_c is the number concentration of cloud droplets (m^{-3}) and nint(x) refers to the nearest integer of x; μ_c is not set to a constant value.

The analytic integration of (8) can be done if the terminal velocities and collection efficiency in the collection kernel $K(R, r)$ are described using polynomials or gamma distribution functions of R and r. The terminal velocity of cloud droplets is given by $v_{t,c} = v_{0,c} r^2$, following Stokes' law, and this expression agrees well with the terminal velocity obtained empirically by Beard (1976), which is considered as one of the most precise approximations (Pruppacher and Klett 1997; Khain and Pinsky 2018) (Fig. 1a). The terminal velocity of graupel particles is given by $v_{t,g} = v_{0,g} R^{\gamma_g}$, where $v_{0,g}$ and γ_g are determined using the terminal velocity data of Khain et al. (2001) (Fig. 1b). The determined values of $v_{0,c}$, $v_{0,g}$, and γ_g are $1.097\,34 \times 10^8$, 776, and 0.84, respectively, when $v_{t,c}$ and $v_{t,g}$ are in meters per second and r and R are in meters. Because the terminal velocities of cloud droplets and graupel particles increase as the air density decreases, the

TABLE 1. Coefficients for the fitted collision efficiency obtained using the collision efficiency data provided by Khain et al. (2001) for various densities of graupel particles.

	Coefficients			
Bulk density ($g\,cm^{-3}$)	b_0 (–)	b_1 (m^{-1})	b_2 (m^{-1})	b_3 (m^{-1})
0.1	1	488 040	1626	18 360
0.4	1	680 227	2471	65 603
0.8	1	857 050	3563	92 093

density factor $(\rho_0/\rho)^{1/2}$ is additionally multiplied to the terminal velocities.

Khain et al. (2001) calculated the collision efficiency between cloud droplets and graupel particles of various sizes using a particle trajectory model. In this study, the collection efficiency is determined as an exponential function to fit the collision efficiency data for graupel particles with a bulk density of $0.4\,g\,cm^{-3}$ obtained by Khain et al. (2001):

$$\eta = b_0[1 - \exp(-b_1 r)][1 - \exp(-b_2 R - b_3 r)]. \quad (10)$$

The determined values of b_0, b_1, b_2, and b_3 are 1, $680\,227\,m^{-1}$, $2471\,m^{-1}$, and $65\,603\,m^{-1}$, respectively. Although the collision efficiency data for graupel particles with bulk densities of 0.1 and $0.8\,g\,cm^{-3}$ are also provided by Khain et al. (2001), the data for the bulk density of graupel particles of $0.4\,g\,cm^{-3}$, which is typically employed in many bulk microphysics schemes (Morrison et al. 2005; Milbrandt and Yau 2005; Thompson et al. 2008), are used in this study. The fitting coefficients for the other densities of graupel particles are given in Table 1. Unlike the bulk collection efficiency used in most bulk microphysics schemes, the collection efficiency used in this study is expressed as a function of the pair of individual graupel particle and cloud droplet. Attributable to the challenges involved in describing flow fields around particles for high Reynolds numbers, Khain et al. (2001) calculated the collision efficiency of graupel particles smaller than 400 μm with the bulk density of $0.4\,g\,cm^{-3}$. The collision efficiency of Khain et al. (2001) approaches 1 as the sizes of cloud droplet and graupel particle increase. In addition, they presented a minimum cloud droplet size, below which cloud droplets are not collected by graupel particles because of the influence of the velocity field induced by graupel particles; for example, a graupel particle with radius 300 μm cannot collect cloud droplets with radii below 3 μm. The bin microphysics scheme of the Hebrew University Cloud Model (HUCM; Khain et al. 2011) that also adopts the collision efficiency of Khain et al. (2001) extrapolates the collision efficiency to graupel particles larger than 400 μm assuming that the minimum cloud droplet size also exists for larger graupel particles. The extrapolated collision efficiency may gradually deviate from reality as graupel particles grow larger. However, the number of very large graupel particles is usually very small; thus, the deviation hardly affects the accretion rate. The extrapolated collision efficiency used in this study is identical to that in the HUCM, and it is used to determine the fitted collision efficiency. Figure 2 shows that overall the fitted collision efficiency agrees well with the collision efficiency of Khain et al. (2001), including the extrapolation to large graupel particles. Although the collision efficiency is overestimated for very small cloud droplets, the contribution of such cloud droplets to the accretion rate is negligible because the gamma size distribution, (9b), reflects that very small cloud droplets are few.

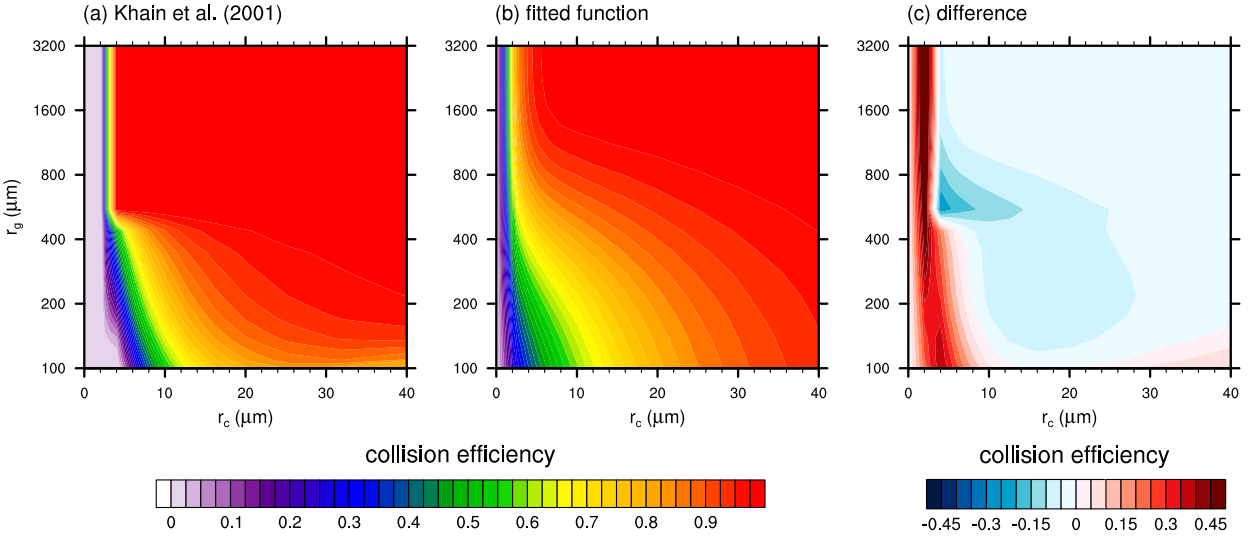

FIG. 2. Collision efficiency between graupel particles and cloud droplets (a) from the particle trajectory model and (b) the fitted function. (c) The fitted collision efficiency minus the collision efficiency obtained by Khain et al. (2001).

Once the terminal velocities and collection efficiency are determined, the collection kernel, (5), is obtained. Compared to the collection kernel calculated directly from the terminal velocities of Beard (1976) and Khain et al. (2001) and the collision efficiency of Khain et al. (2001), the collection kernel obtained in this study shows good agreement (not shown). Note that the directly calculated collection kernel is used in the bin microphysics scheme (Khain et al. 2011).

The absolute value in (5) makes the integral in (8) challenging to solve analytically. In this study, the absolute value of the terminal velocity difference is approximated as the terminal velocity difference itself as in Gaudet and Schmidt (2005) because the contribution of the part in which cloud droplets fall faster than graupel particles to the integral is very small. This approximation is confirmed to hardly change the accretion rate in box model simulations performed using a bin-based SCE solver.

Using the obtained collection kernel and the size distributions of graupel particles and cloud droplets, the accretion rate is expressed as follows:

$$\left.\frac{\partial L_g}{\partial t}\right|_{\text{acc}} = \frac{4}{3}\pi^2\rho_w\left(\frac{\rho_0}{\rho}\right)^{1/2} N_{0,g}N_{0,c}b_0(v_{0,g}L_1 - v_{0,c}L_2), \quad (11)$$

where

$$L_1 = \sum_{i=0}^{2} a_i\{\Gamma_1(\lambda_g, 3+\gamma_g - i)[\Gamma_1(\lambda_c, \mu_c + 4 + i) - \Gamma_1(\lambda_c + b_1, \mu_c + 4 + i)] - \Gamma_1(\lambda_g + b_2, 3 + \gamma_g - i)[\Gamma_1(\lambda_c + b_3, \mu_c + 4 + i) - \Gamma_1(\lambda_c + b_1 + b_3, \mu_c + 4 + i)]\}, \quad (12a)$$

$$L_2 = \sum_{i=0}^{2} a_i\{\Gamma_1(\lambda_g, 3 - i)[\Gamma_1(\lambda_c, \mu_c + 6 + i) - \Gamma_1(\lambda_c + b_1, \mu_c + 6 + i)] - \Gamma_1(\lambda_g + b_2, 3 - i)[\Gamma_1(\lambda_c + b_3, \mu_c + 6 + i) - \Gamma_1(\lambda_c + b_1 + b_3, \mu_c + 6 + i)]\}. \quad (12b)$$

Here, a_i is given as $(a_0, a_1, a_2) = (1, 2, 1)$, and $\Gamma_1(\lambda, s)$ is defined as

$$\Gamma_1(\lambda, s) = \frac{\Gamma(s)}{\lambda^s}, \quad (13)$$

where $s > 0$. Because of mass conservation, the following relation is satisfied:

$$\left.\frac{\partial L_c}{\partial t}\right|_{\text{acc}} = -\left.\frac{\partial L_g}{\partial t}\right|_{\text{acc}}. \quad (14)$$

In a similar way, the tendency of cloud droplet number concentration can be evaluated by integrating the following equation:

$$\left.\frac{\partial N_c}{\partial t}\right|_{\text{acc}} = \int_0^\infty\int_0^\infty f_g(R)K(R,r)f_c(r)\,dr\,dR. \quad (15)$$

Equation (15) is finally expressed as follows:

$$\left.\frac{\partial N_c}{\partial t}\right|_{\text{acc}} = -\pi N_{0,g}N_{0,c}b_0(v_{0,g}N_1 - v_{0,c}N_2), \quad (16)$$

where

$$N_1 = \sum_{i=0}^{2} a_i\{\Gamma_1(\lambda_g, 3+\gamma_g - i)[\Gamma_1(\lambda_c, \mu_c + 1 + i) - \Gamma_1(\lambda_c + b_1, \mu_c + 1 + i)] - \Gamma_1(\lambda_g + b_2, 3 + \gamma_g - i)[\Gamma_1(\lambda_c + b_3, \mu_c + 1 + i) - \Gamma_1(\lambda_c + b_1 + b_3, \mu_c + 1 + i)]\}, \quad (17a)$$

$$N_2 = \sum_{i=0}^{2} a_i\{\Gamma_1(\lambda_g, 3 - i)[\Gamma_1(\lambda_c, \mu_c + 3 + i) - \Gamma_1(\lambda_c + b_1, \mu_c + 3 + i)] - \Gamma_1(\lambda_g + b_2, 3 - i)[\Gamma_1(\lambda_c + b_3, \mu_c + 3 + i) - \Gamma_1(\lambda_c + b_1 + b_3, \mu_c + 3 + i)]\}. \quad (17b)$$

The graupel number concentration is not affected by the accretion process.

4. Box model results

The developed accretion parameterization is evaluated using a box model in which only collision between graupel particles and cloud droplets is considered. As in double-moment bulk microphysics schemes, the mass and number concentrations of the hydrometeor species are predicted in the box model. During the accretion process, cloud water mass is converted into graupel mass as time passes. For comparison, the aforementioned

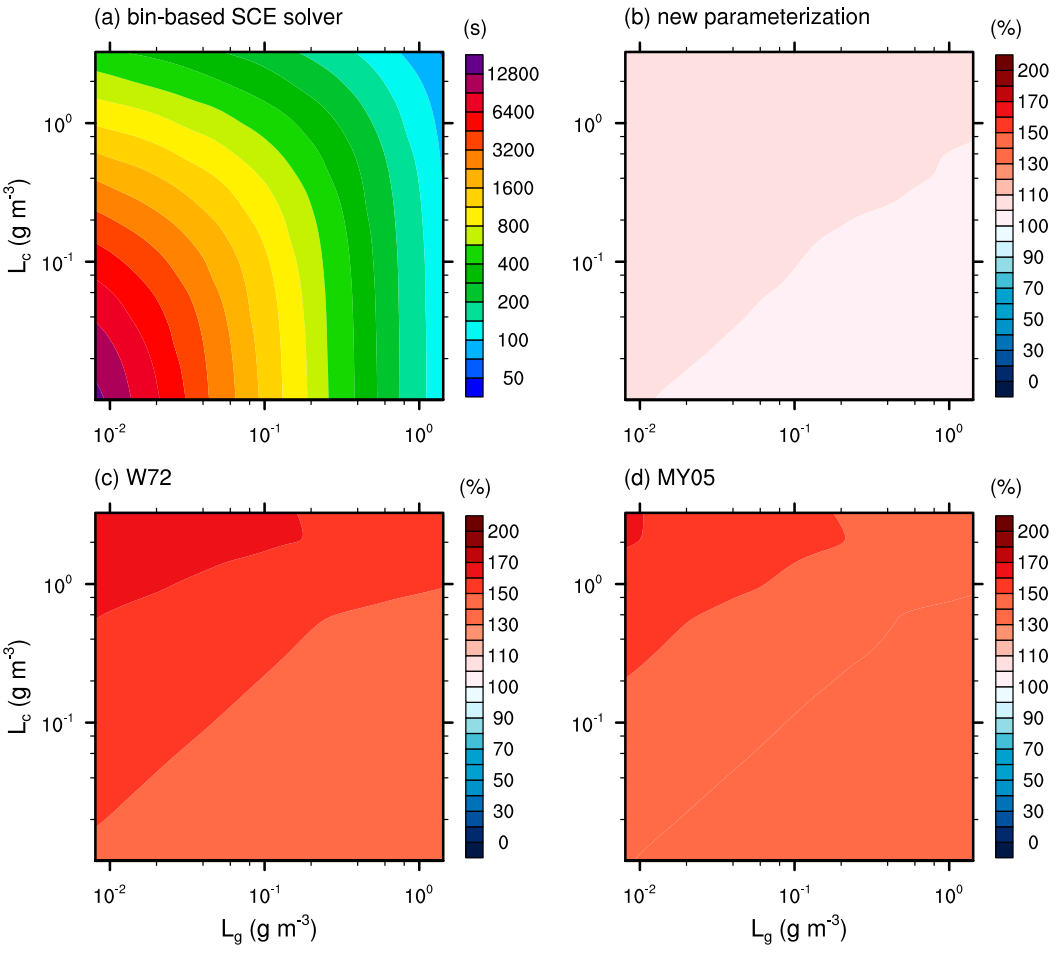

FIG. 3. Time required for 50% of the initial cloud water mass content to be converted into graupel mass content via accretion t_{50} as a function of the initial cloud water mass content and the initial graupel mass content (a) from the bin-based solver used as reference and percentage ratios of t_{50} against reference obtained using (b) the new parameterization, (c) W72, and (d) MY05.

accretion parameterizations W72 and MY05 are also tested using the box model. Both W72 and MY05 parameterizations use the bulk collection efficiency suggested by Cober and List (1993). As a reference, a bin-based direct SCE solver used in Lee and Baik (2017) is modified to simulate the accretion process and implemented in the box model. The solver uses 43 mass-doubling bins for liquid drops and graupel particles. The radius of the smallest liquid drops is 2 μm. The initial size distributions of the hydrometeor species follow (9a) and (9b), but the size distributions are not confined to those functions after the model integration begins. The time step is set to 1 s. Wide ranges of the initial mass contents and number concentrations are applied (i.e., 0.01–3.3 g m^{-3} for the cloud water mass content, 1–2000 cm^{-3} for the cloud droplet number concentration, 0.008–3.2 g m^{-3} for the graupel mass content, and 0.0001–0.02 cm^{-3} for the graupel number concentration).

This study uses t_{50}, the time required for 50% of the initial cloud water mass content to be converted into graupel mass content because of the accretion process, to evaluate accuracy of accretion parameterizations. Figure 3 shows t_{50} obtained from the bin-based solver that is used as reference and percentage ratios of t_{50} against reference obtained using the new parameterization, W72, and MY05. The initial mass-weighted radii of graupel particles and cloud droplets are fixed at 800 and 15 μm, respectively, and t_{50} is obtained for various initial graupel and cloud water mass contents (120 simulations for each of the accretion parameterizations and the bin-based SCE solver). The overall shape of the variation in t_{50} for different initial hydrometeor mass contents in the direct SCE solver is well captured by all the three accretion parameterizations. However, W72 and MY05 overestimate t_{50} by 45%–69% and 36%–61%, respectively, compared to the direct SCE solver

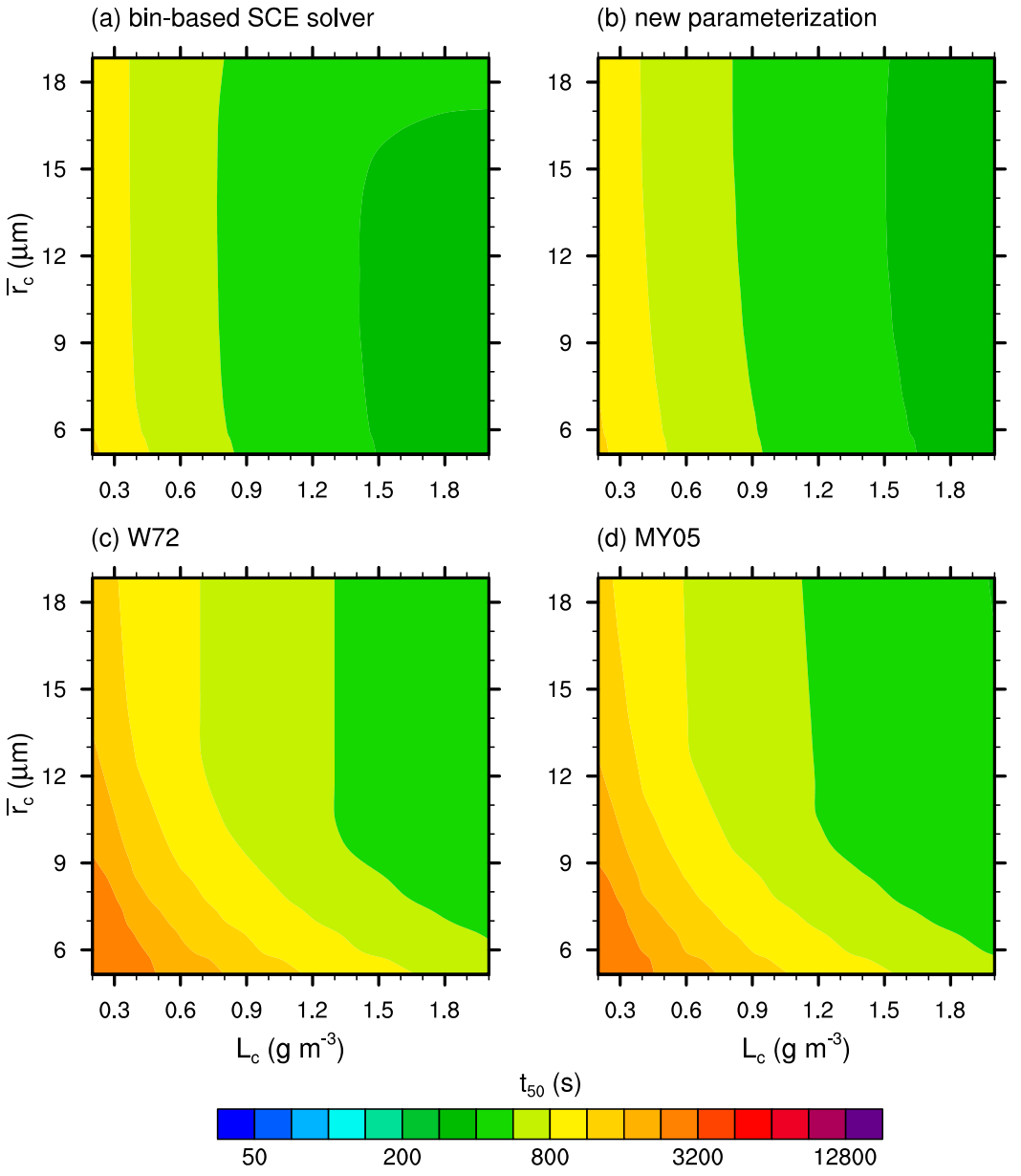

FIG. 4. Plots of t_{50} as a function of the initial cloud water mass content and the initial mass-weighted mean radius of cloud droplets obtained using (a) the bin-based SCE solver, (b) the new parameterization, (c) W72, and (d) MY05.

(i.e., both of them predict slower accretion compared to the direct SCE solver). The degree of overestimation gets larger as the initial cloud water mass content increases and the initial graupel mass content decreases. In contrast, the new parameterization predicts values of t_{50} that are very similar to those of the direct SCE solver; it overestimates t_{50} by only 4%–7%. One possible reason for the difference in t_{50} between the new parameterization and the bin-based SCE solver is the deviation of the particle size distributions in the bin-based SCE solver from the gamma and exponential size distributions assumed in the new parameterization (not shown).

The advantage of the new accretion parameterization is particularly remarkable when the mean size of collected cloud droplets is relatively small. Figure 4 shows t_{50} as a function of the initial cloud water mass content and the initial mass-weighted mean radius of cloud droplets $\overline{r}_c$ when the corresponding values for graupel are fixed at 0.1 g m^{-3} and 800 μm, respectively. Only the

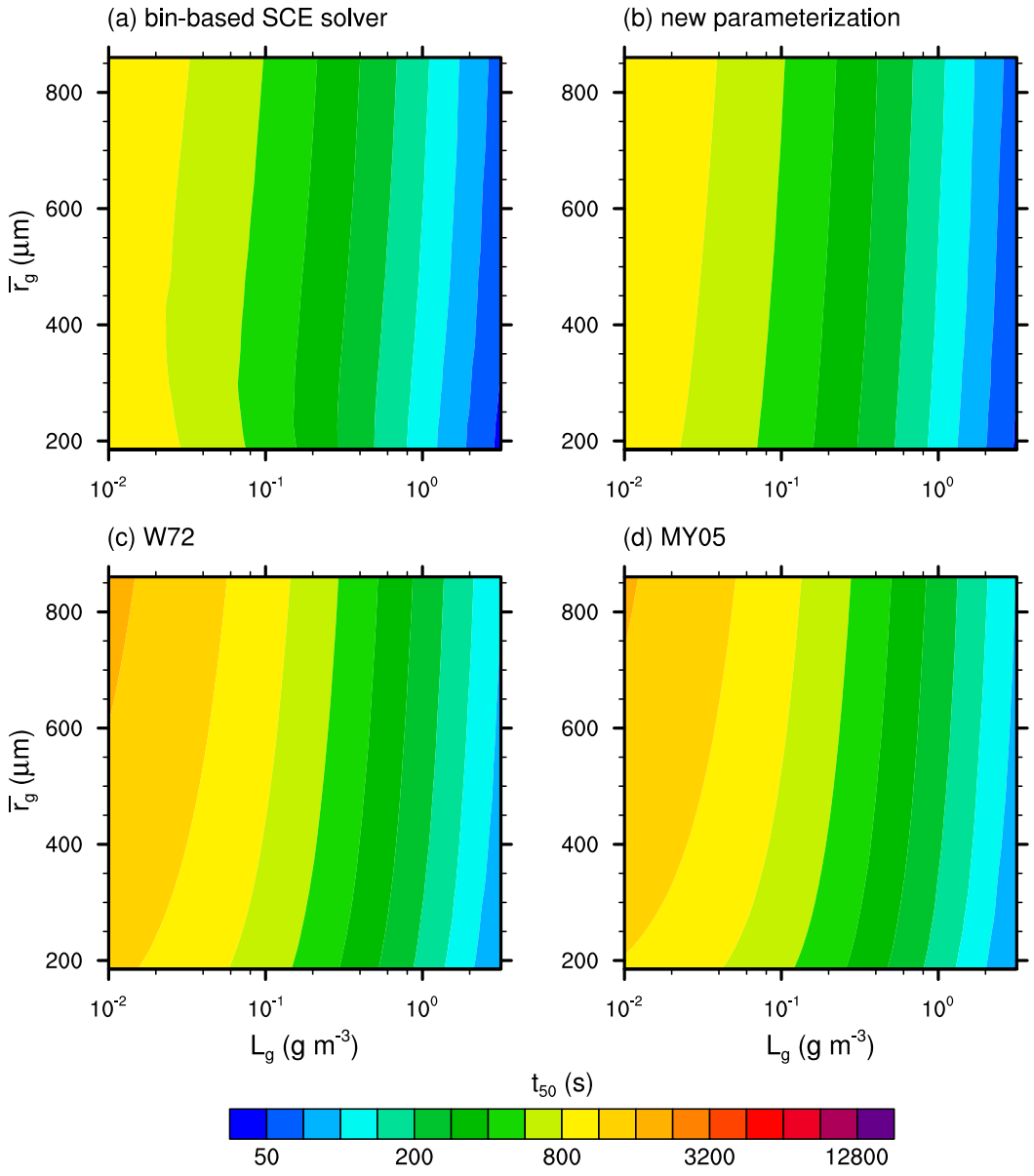

FIG. 5. As in Fig. 4, but as a function of the initial graupel mass content and the initial mass-weighted mean radius of graupel particles.

new parameterization predicts t_{50} values very close to those predicted by the direct SCE solver. W72 and MY05 significantly overestimate t_{50}. Furthermore, W72 and MY05 predict large increases in t_{50} with decreasing $\overline{r}_c$ when the mean cloud droplet size is small; this behavior is not predicted by the direct SCE solver. One possible reason is that the parameterization of Cober and List (1993) used in W72 and MY05 may underestimate the bulk collection efficiency for small $\overline{r}_c$. Because the bulk collection efficiency is parameterized using only the median volume radius of cloud droplets and the mass-weighted mean radius and terminal velocity of graupel particles, the effects of other factors that may influence the bulk collection efficiency, such as possible differences in the size distribution of cloud droplets, are not considered. This observation suggests that the collection efficiency should be described as a function of the radii of individual colliding particles.

Figure 5 shows t_{50} as a function of the initial graupel mass content and the initial mass-weighted mean radius of graupel when the corresponding values for cloud droplets are fixed at $1\,\mathrm{g\,m^{-3}}$ and $15\,\mu\mathrm{m}$, respectively. The overall overestimation of t_{50} in W72 and MY05

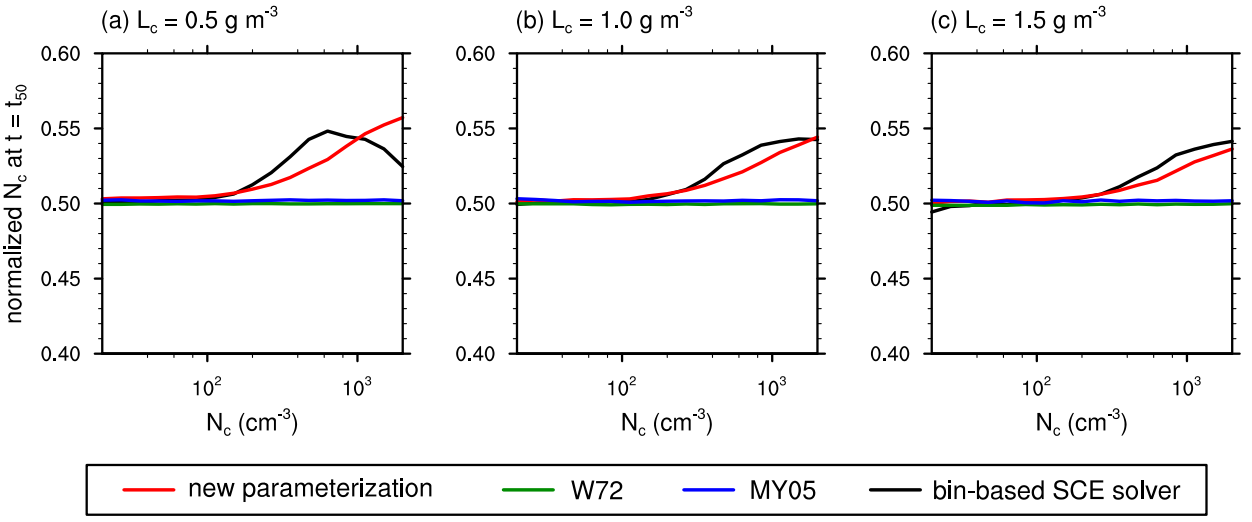

FIG. 6. Cloud droplet number concentration at $t = t_{50}$ normalized by its initial value as a function of the initial cloud droplet number concentration obtained using different accretion parameterizations and the bin-based direct SCE solver. The initial cloud water mass contents are (a) 0.5, (b) 1.0, and (c) 1.5 g m^{-3}.

compared to the direct SCE solver again appears, whereas the new parameterization agrees well with the direct SCE solver. The changes in t_{50} with respect to the mass content and mean radius of graupel particles in all three accretion parameterizations are well matched to the change in the direct SCE solver except when the initial graupel particles are small.

The ability of the accretion parameterizations to predict accretion-driven changes in the cloud droplet number concentration is evaluated. Figure 6 shows the cloud droplet number concentration at $t = t_{50}$ normalized by its initial value as a function of the initial cloud droplet number concentration for different initial cloud water mass contents. The result produced by W72 is 0.5, regardless of initial cloud droplet number concentrations and cloud water mass contents, revealing that the proportional reduction in the cloud droplet number concentration due to the accretion process is exactly the same as that of the cloud water mass content when the continuous collection concept is adopted. However, the direct SCE solver predicts smaller reductions in the cloud droplet number concentration when its initial value exceeds $\sim$100 cm^{-3}. This result is more realistic because the number concentration of small cloud droplets, which have smaller collision efficiencies, decreases more slowly than that of large cloud droplets. Thus, because the total number concentration of cloud droplets is generally dominated by small cloud droplets, it decreases more slowly than the cloud water mass content. The new parameterization captures this feature quite well, especially when the cloud water mass content is large. Although MY05 partly represents the variation in the probability of collision with respect to the sizes of cloud droplets through changes in the swept volume, the results do not deviate greatly from those obtained using continuous collection (W72), which is attributable to the use of the bulk collection efficiency.

Given the results of the box model simulations, the new accretion parameterization shows its advantages; changes in cloud water mass content, graupel mass content, and cloud droplet number concentration and their dependences on the initial mass contents and number concentrations of the hydrometeor species predicted by the new parameterization are closest to those predicted by the direct SCE solver. In addition, the new accretion parameterization predicts decreases in the cloud droplet number concentration that are slower than those predicted by the other bulk accretion parameterizations, consistent with the direct SCE solver. This improvement of the prediction can be achieved with a small additional investment of computational resources because a large part of the calculation in (12) and (17) can be prepared before the start of time integration. Moreover, in cloud-resolving model simulations, the difference in computation time between the new parameterization and W72 becomes very small because the accretion of cloud water by graupel is only one of the numerous microphysical processes considered in the model.

5. Cloud-resolving model results

a. Idealized simulations

To perform cloud-resolving simulations, the new accretion parameterization is implemented in a cloud-resolving

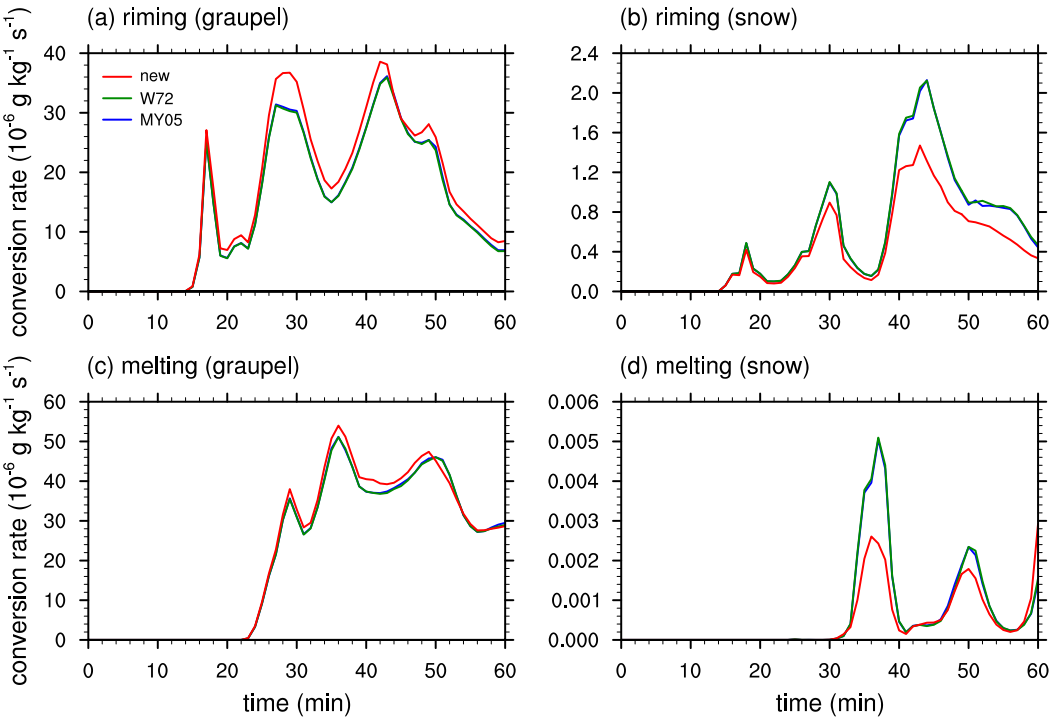

FIG. 7. Time series of the domain-averaged conversion rates by (a) riming of graupel, (b) riming of snow, (c) melting of graupel, and (d) melting of snow with different accretion parameterizations.

model. The WRF Model, version 3.8.1 (Skamarock et al. 2008), and the Thompson–Eidhammer microphysics scheme (Thompson and Eidhammer 2014) are used. The new parameterization, W72, and MY05 are used to represent the accretion process in the Thompson–Eidhammer microphysics scheme. Note that the Thompson–Eidhammer microphysics scheme originally adopts W72 as accretion parameterization. Except for the accretion of cloud water by graupel, the other microphysical processes including the accretion of cloud water by rain and snow in the Thompson–Eidhammer microphysics scheme are unchanged. It is also noted that in the cloud-resolving model simulations in this study, the differences in the accretion parameterizations cause the differences in the simulated flows, and they both contribute to the differences between the results of the simulations with the different accretion parameterizations.

To simulate deep convective clouds where graupel and cloud water coexist, a thermodynamic sounding is adopted from Weisman and Klemp (1982). The water vapor mixing ratio near the surface is set to 14 g kg^{-1}, and no basic wind is considered. The horizontal domain size is 90 km × 90 km with a constant grid spacing of 300 m. At lateral boundaries, periodic boundary conditions are applied in both directions. The vertical domain size extends to 20 km with a grid spacing of ~200 m. The sponge layer is located from z = 15 km to the domain top. The model is integrated for 1 h, and the time step is 2 s. An axially symmetric initial thermal perturbation (a warm bubble) is applied. The cloud condensation nuclei (CCN) and ice nuclei are considered in the simulations, and their number concentrations exponentially decrease with height. The CCN concentration near the surface is 2000 cm^{-3}.

Figure 7 shows time series of the domain-averaged conversion rates, and Fig. 8 shows time series of the domain-averaged mixing ratios of hydrometeor species and the surface precipitation rate obtained using the different accretion parameterizations. A 60 km × 60 km × 15 km domain that has the horizontal center that is the same as that of the simulation domain and vertically extends up to 15 km above ground level is used to calculate the domain-averaged values. Note that the graupel and snow riming shown in Figs. 7a and 7b is dominated by the accretion of cloud water by graupel and snow, respectively (not shown). W72 and MY05 show very similar results in these 1-h simulations. The graupel riming rate predicted by the new parameterization is larger than that predicted by W72 and MY05 because of the efficient accretion of cloud water by graupel, which is also

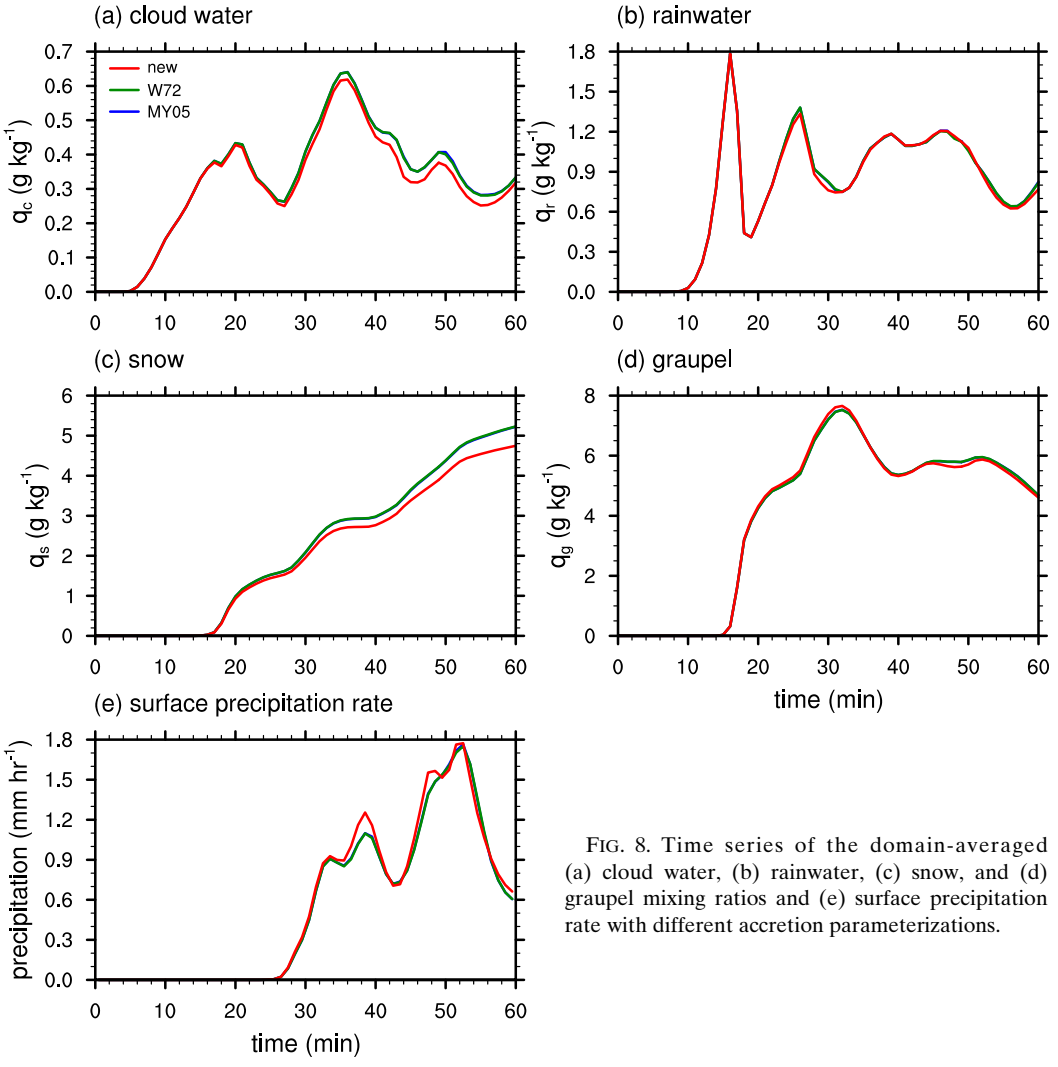

FIG. 8. Time series of the domain-averaged (a) cloud water, (b) rainwater, (c) snow, and (d) graupel mixing ratios and (e) surface precipitation rate with different accretion parameterizations.

shown in the box model simulations. As a result, in the new parameterization, a greater amount of cloud water is accreted by graupel, and the cloud water mixing ratio is smaller (Fig. 8a). The greater amount of graupel production leads to a greater amount of melting of graupel (Fig. 7c). In contrast, the snow riming rate in the new parameterization is smaller than that in W72 and MY05 mainly because the mixing ratio of the collected cloud water is smaller. Although the snow riming rate is much smaller than the graupel riming rate because of the less efficient collection by snow, the difference in the snow riming rate leads to a noticeable difference in the snow mixing ratio as the model integration progresses (Fig. 8c). At $t = 60$ min, the snow mixing ratio in W72 is approximately 10% larger than that in the new parameterization. The snow melting rate is larger in W72 than in the new parameterization (Fig. 7d). However, most of the snow formed above the freezing level does not fall below the freezing level in the 1-h model integration time because of its relatively slow sedimentation process, which makes the snow melting rate negligible compared to the graupel melting rate. Hence, the surface precipitation is dominated by rain produced by the melting of graupel. Consequently, the new parameterization predicts the largest surface precipitation rate over most of the model integration time (Fig. 8e).

Figures 7a and 8d show that the increase in the graupel riming rate does not lead to the increase in the graupel mixing ratio. One reason is that the melting of graupel also increases, but there are other reasons as well. Because graupel particles, snow particles, and raindrops compete with each other to collect cloud droplets, the increase in the accretion of cloud water by graupel induces the decrease in the accretion of

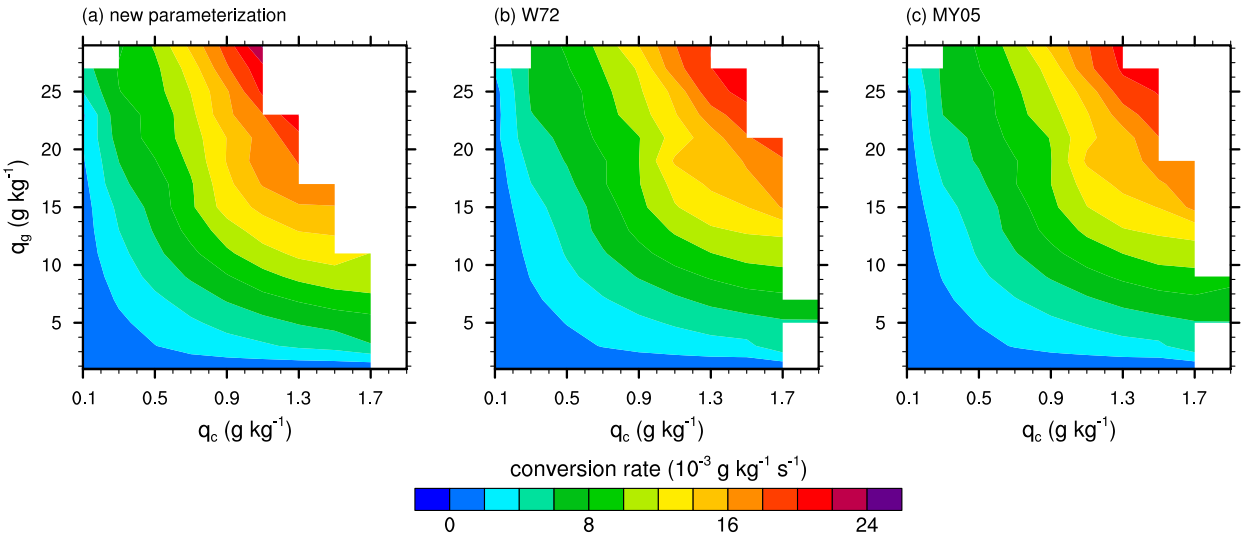

FIG. 9. Averaged accretion rates as a function of cloud water mixing ratio and graupel mixing ratio obtained using (a) the new parameterization, (b) W72, and (c) MY05.

cloud water by rain and snow. The decrease in the rain and snow production leads to the decrease in graupel production by microphysical processes other than the riming of graupel, such as the freezing of raindrops and the collision between raindrops and snow particles that produces graupel. This negative feedback reduces the differences in the hydrometeor amounts caused by the different parameterizations of the accretion of cloud water by graupel.

Figure 9 shows the averaged accretion rate as a function of the cloud water mixing ratio and graupel mixing ratio. The cloud water mixing ratio and the graupel mixing ratio are divided into multiple intervals, and the accretion rates at the grid points that correspond to each pair of mixing ratio intervals are averaged. In the new accretion parameterization, relatively small graupel and cloud water mixing ratios are sufficient to cause active accretion, compared to W72 and MY05. The maximum accretion rate appears when the cloud water mixing ratio is $\sim$1.1 g kg^{-1} in the new parameterization, $\sim$1.5 g kg^{-1} in W72, and $\sim$1.5 g kg^{-1} in MY05. The new parameterization shows the largest sensitivity of the accretion rate to the cloud water mixing ratio for a given graupel mixing ratio.

b. *Real-case simulations*

To evaluate the performance of the new accretion parameterization in simulating clouds and precipitation, a real precipitation event is simulated using the three different accretion parameterizations. The precipitation event occurred on 14–15 March 2018 over the southern Korean Peninsula. The maximum 24-h accumulated surface precipitation amount observed by automatic weather stations (AWSs) operated by the Korea Meteorological Administration (KMA) was 119 mm. A synoptic trough passed over the Korean Peninsula from the west to the east, and southwesterly winds transported water vapor from the ocean. These features favored the development of a precipitation band moving eastward.

Figure 10 shows the model domain configuration. Three domains with one-way nesting are used; these domains have horizontal grid spacings of 27, 9, and 3 km. The number of horizontal grids in domains 1, 2, and 3 is 150 $\times$ 120, 217 $\times$ 178, and 241 $\times$ 262, respectively. The domain includes 42 vertical layers, and the vertical grid spacing increases with height from $\sim$60 m in the lowest layer to $\sim$600 m in the highest layer. The model-top height is $\sim$20 km (50 hPa). The physics parameterizations used for the simulations are the Yonsei University (YSU) planetary boundary layer scheme (Hong et al. 2006), the Kain–Fritsch cumulus parameterization scheme (Kain 2004), the Dudhia shortwave radiation scheme (Dudhia 1989), the Rapid Radiative Transfer Model (RRTM) longwave radiation scheme (Mlawer et al. 1997), the unified Noah land surface model (Tewari et al. 2004), and the MM5 similarity surface-layer scheme (Zhang and Anthes 1982). The cumulus parameterization scheme is applied only to domains 1 and 2. The model integration is performed for 24 h starting from 1500 LST 14 March 2018. The simulation data of the last 12 h in a selected domain where the precipitation was the

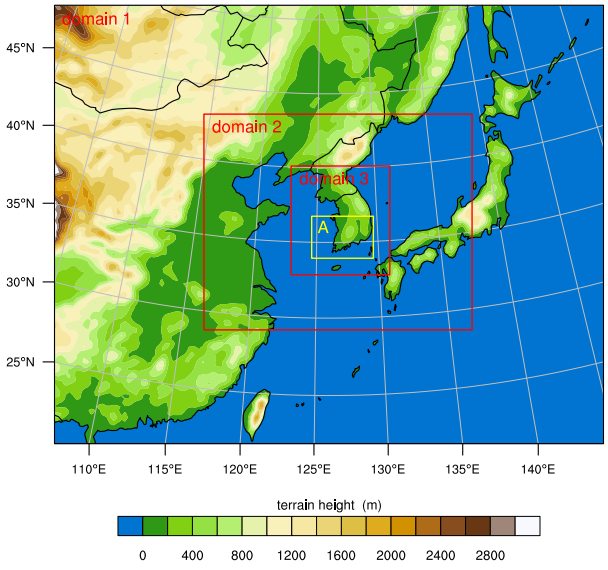

FIG. 10. Illustration of three nested model domains with terrain height. The yellow box corresponds to the analysis domain.

most intense (yellow box in Fig. 10) are analyzed in this study. National Centers for Environmental Prediction (NCEP) final analysis data (NCEP 2015), which have a horizontal resolution of 0.25° and a time interval of 6 h, are used for boundary conditions for the outermost domain and initial conditions. The initial and boundary aerosol data are obtained from multiyear global model simulations (Colarco et al. 2010; Thompson and Eidhammer 2014). The synoptic patterns simulated using the new parameterization, W72, and MY05 are similar to observations (not shown).

Table 2 lists the Brier scores of the results obtained using the different accretion parameterizations. The Brier score is calculated by matching the 12-h accumulated precipitation amount predicted in an area around each observation point, which is called the ''neighborhood,'' to that at the observation point. This ''single observation–neighborhood forecast'' technique allows slight displacements in the forecasts. A detailed description of this technique is provided in Ebert (2008). As the observation points, 251 AWSs located inside the yellow box in Fig. 10 are used. When matching one grid to an observation point, the new parameterization shows the lowest Brier scores, which correspond to the best performance, for all precipitation thresholds. Especially, the prediction for a threshold of 40 mm in the new parameterization is much better than in the other accretion parameterizations. W72 shows a level of performance similar to the new parameterization in simulating large

TABLE 2. Brier scores calculated using 1 × 1 and 11 × 11 grids surrounding the AWSs. The lowest Brier score among the three accretion parameterizations for each precipitation threshold and number of grid points surrounding the AWSs is given in boldface.

		Precipitation threshold (mm)		
Grid points	Parameterization	20	40	60
1 × 1				
	New	**0.283**	**0.255**	**0.159**
	W72	0.291	0.299	**0.159**
	MY05	0.287	0.307	0.175
11 × 11				
	New	**0.189**	**0.234**	0.117
	W72	0.204	0.254	0.113
	MY05	0.215	0.263	**0.109**

accumulated precipitation amount. When the matched area in the simulation results is enlarged, the Brier score for a threshold of 20 mm as well as that for a threshold of 40 mm is noticeably lower in the new parameterization than in the other accretion parameterizations, although MY05 best predicts the accumulated precipitation amount for a threshold of 60 mm.

Figure 11 shows the longitude–time section of the surface precipitation rate and the differences in latitude-averaged surface precipitation amounts between the new and other parameterizations. During the simulations, the precipitation bands move eastward. The movements of the precipitation bands simulated using the different accretion parameterizations are similar to each other, but the distributions of the precipitation rate are different. In the new parameterization, the regions of high precipitation rates (reddish area in Fig. 11) are temporally and spatially concentrated compared to W72. In the new parameterization and MY05, the regions of high precipitation rates appear mostly between ~0700 and ~0900 LST. Compared to the other accretion parameterizations, the new parameterization predicts larger amounts of surface precipitation in the west-central region (~126.3°–127.2°E) and smaller amounts of surface precipitation in the east-central region (~127.2°–127.7°E), shifting the surface precipitation to the upwind side (Fig. 11d).

Figure 12 shows the fractions of precipitation amounts that belong to three different precipitation-rate categories: light ($<10\,\mathrm{mm\,h^{-1}}$), moderate ($10–30\,\mathrm{mm\,h^{-1}}$), and heavy ($\geq 30\,\mathrm{mm\,h^{-1}}$). Because the history interval of the model output is 5 min, 5-min accumulated precipitation amounts are categorized by their corresponding precipitation rates and summed up.

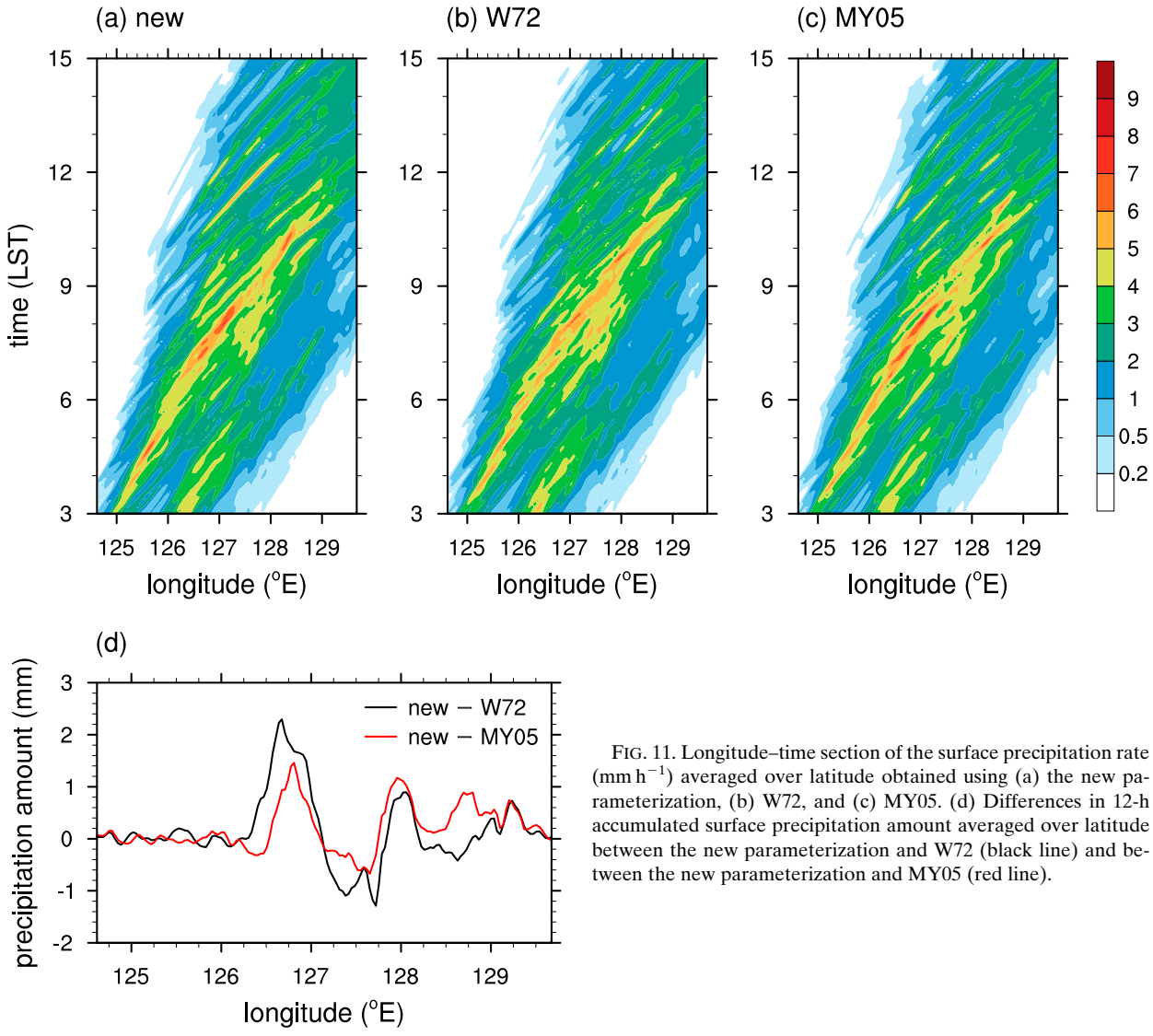

FIG. 11. Longitude–time section of the surface precipitation rate (mm h^{-1}) averaged over latitude obtained using (a) the new parameterization, (b) W72, and (c) MY05. (d) Differences in 12-h accumulated surface precipitation amount averaged over latitude between the new parameterization and W72 (black line) and between the new parameterization and MY05 (red line).

W72 predicts the largest fraction of moderate precipitation amount and the smallest fraction of heavy precipitation amount. In contrast, the new parameterization predicts the smallest fractions of light and moderate precipitation amounts and the largest fraction of heavy precipitation amount. The fraction of heavy precipitation amount in the new parameterization is ~1.11 times that in W72.

As in section 5a, time series of domain-averaged conversion rates and hydrometeor mixing ratios with the different accretion parameterizations are shown in Fig. 13. One key difference relative to the idealized simulations is that the environment in this real case is snow dominant. The domain-averaged snow mixing ratio is more than 10 times the domain-averaged graupel mixing ratio (Figs. 13e,f). As a result, the differences in the snow mixing ratio and the microphysical processes related to snow as well as those for graupel among the three different simulations may significantly affect the precipitation process. In the new parameterization, the riming rate, mixing ratio, and melting rate of graupel are mostly greater than those in the other parameterizations. None of the accretion parameterizations consistently shows the greatest riming or melting rate of snow. Since the melting rate of graupel is much smaller than the melting rate of snow, the greater melting rate of graupel does not make a significant difference in the domain-averaged surface precipitation rate (not shown). However, the differences in the graupel- and snow-related microphysical processes can change the spatial and

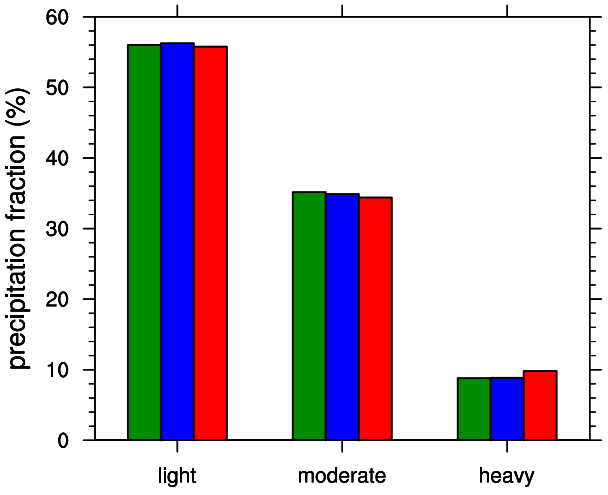

FIG. 12. Precipitation fractions of three different precipitation-rate categories obtained using the new parameterization (red), W72 (green), and MY05 (blue). The surface precipitation rates are categorized into light ($<10\,\text{mm h}^{-1}$), moderate ($10–30\,\text{mm h}^{-1}$), and heavy ($\geq 30\,\text{mm h}^{-1}$).

temporal distribution of the precipitation, as will be discussed later.

Figure 14 shows vertical profiles of each hydrometeor mixing ratio obtained using the new parameterization and the differences in hydrometeor mixing ratio and heating rate between the new parameterization and W72 averaged over $t = 0700–0900$ LST 15 March 2018, when the precipitation was the most intense (see Fig. 11). Snow composes the largest mass of the clouds, and its maximum mixing ratio appears at $z \sim 4.5$ km. The maximum mixing ratio of graupel appears at $z \sim 3$ km, and that of rainwater appears at $z \sim 2$ km. The main differences between the new parameterization and W72 are the larger graupel mixing ratio and smaller snow mixing ratio in the region $z \sim 2–7$ km and the larger snow mixing ratio in the region $z > \sim 7$ km in the new parameterization (Fig. 14b). Because of the greater riming rate of graupel in the new parameterization, a larger amount of graupel is produced and the riming of snow is weakened in the region $z \sim 3–5$ km. In addition, because the new parameterization predicts a slower decrease in the cloud droplet number concentration via accretion than W72, the cloud droplets transported upward have a smaller mean radius than W72. This reduces the collection efficiency between snow and cloud water and further hinders the growth of snow. The reduced production of snow is followed by the decrease in snow deposition in the middle level (Fig. 14c). The unconsumed water vapor is transported to the higher level, which makes the larger amount of snow in the higher level via deposition or freezing of condensed cloud water. The smaller snow mixing ratio in the new parameterization induces the weaker riming and melting of snow. The large heating rate difference by melting in the region $z \sim 2–3$ km is mainly caused by the reduced melting of snow (not shown).

Figure 15 shows horizontal distributions of differences in the updraft velocity greater than $0.1\,\text{m s}^{-1}$ in the cloudy areas where the total liquid and ice water mixing ratio is larger than $1\,\text{g kg}^{-1}$, the graupel melting rate, and the snow melting rate at $z = 2$ km between the new parameterization and W72 at $t = 0700$, 0800, and 0900 LST 15 March 2018. The enhanced updrafts in the new parameterization are located in the regions where graupel is abundant. The smaller amount of snow in the new parameterization reduces the melting of snow in relatively wide regions, while the larger amount of graupel in the new parameterization enhances the melting of graupel in relatively narrow regions. Because of the small terminal velocities of snow particles, snow remains aloft for a long time and spreads upward and horizontally, resulting in the relatively wide regions of melting compared to graupel. In contrast, because of the large terminal velocities of graupel particles, graupel is not advected much in the horizontal direction, resulting in the relatively narrow regions of melting compared to snow. As a result, in the new parameterization, the concentrated precipitation is enhanced, and the widespread precipitation is reduced. These differences can explain the larger fraction of heavy precipitation amount and the smaller fractions of light and moderate precipitation amounts in the new parameterization than in W72, as shown in Fig. 12.

6. Summary and conclusions

A new parameterization of the accretion of cloud water by graupel for use in bulk microphysics schemes is derived by analytically integrating the SCE. The collection efficiency of individual graupel particle–cloud droplet pairs obtained from a particle trajectory model by Khain et al. (2001) is used.

Using a box model in which only collision between graupel particles and cloud droplets is allowed, the new parameterization is compared to other accretion parameterizations (W72 and MY05) and a bin-based direct SCE solver. While W72 and MY05 overestimate t_{50} by 45%–69% and 36%–61%, respectively, compared to the direct SCE solver, the new parameterization overestimates t_{50} by only 4%–7%. Furthermore, the dependences of t_{50} on the initial mass contents and number concentrations of

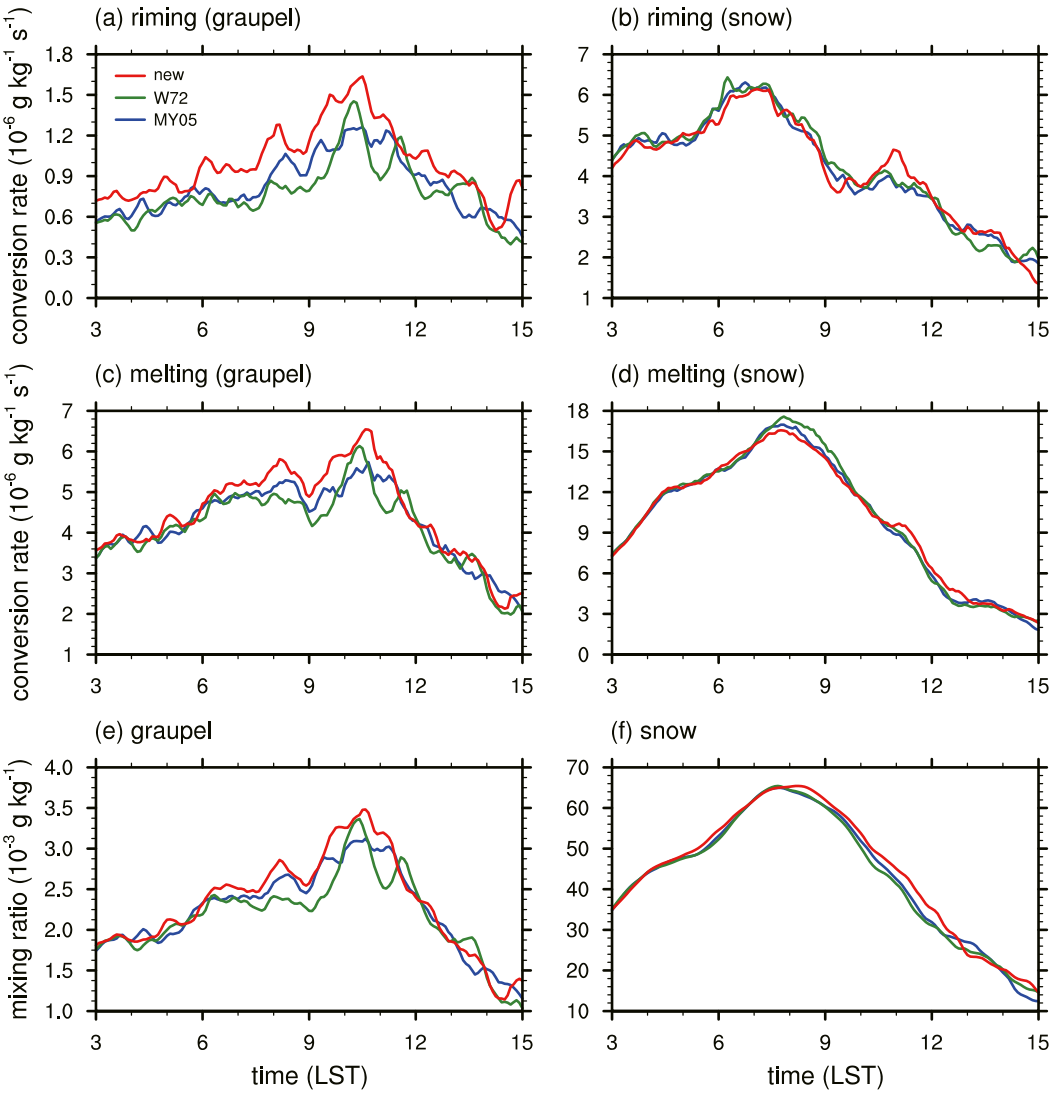

FIG. 13. Time series of the domain-averaged conversion rates by (a) riming of graupel, (b) riming of snow, (c) melting of graupel, and (d) melting of snow and mixing ratio of (e) graupel and (f) snow with different accretion parameterizations.

hydrometeor species in the new parameterization are closest to those in the direct SCE solver compared to the other accretion parameterizations, especially when the mean size of cloud droplets is small. As in the direct SCE solver, a slower decrease in the cloud droplet number concentration is predicted in the new parameterization compared to the other accretion parameterizations. This feature is closer to reality because the number concentration of small cloud droplets with smaller collision efficiencies decreases more slowly than that of large cloud droplets; thus, the total number concentration of cloud droplets decreases more slowly compared to the cloud water mass content.

The new accretion parameterization and the other accretion parameterizations are implemented into a cloud-resolving model that uses the Thompson–Eidhammer microphysics scheme. In the idealized deep convective cloud simulations, the new parameterization predicts the largest rate of accretion by graupel and the smallest rate of accretion by snow; taken together, these enhance rainfall through the largest rate of melting of graupel. In the new parameterization, relatively small amounts of graupel and cloud water are sufficient to lead to active accretion. In the real-case simulations for a precipitation event over the southern Korean Peninsula, the new parameterization shows the best Brier score

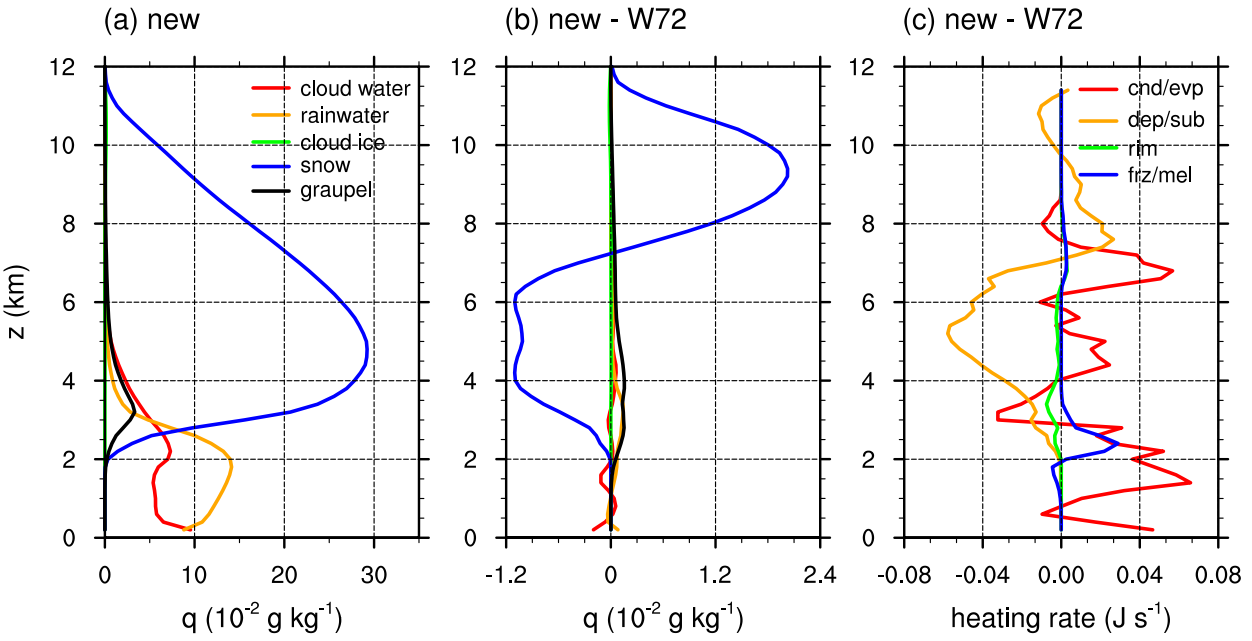

FIG. 14. Domain-averaged vertical profiles of (a) each hydrometeor mixing ratio (cloud water, rainwater, cloud ice, snow, and graupel) obtained using the new parameterization and the differences in (b) each hydrometeor mixing ratio and (c) the heating rate (condensation/evaporation, deposition/sublimation, riming, and freezing/melting) between the new parameterization and W72 averaged over t = 0700–0900 LST 15 Mar 2018. The heating rate is averaged over areas where the total liquid and ice water mixing ratio is larger than 1 g kg^{-1}.

among the accretion parameterizations in the prediction of 12-h accumulated surface precipitation amount. Low-level updrafts are enhanced in the new parameterization. Additionally, the larger amount of graupel produced in the new parameterization enhances the melting of graupel over relatively narrow regions, and the smaller amount of snow produced reduces the melting of snow over relatively wide regions. As a result, the new parameterization reduces the fractions of light and moderate precipitation amounts and enhances the fraction of heavy precipitation amount compared to the other accretion parameterizations.

Unlike the idealized deep convective cloud simulations that favor graupel-dominant clouds, the real-case simulations show snow-dominant clouds, which makes it difficult to directly compare the results of the two sets of simulations. While the new parameterization enhances the surface precipitation in the idealized simulation, it does not enhance the surface precipitation in the real-case simulation but changes the spatial and temporal distribution of the surface precipitation. Further studies of a wide variety of real cases that include graupel-dominant precipitation events as well as snow-dominant precipitation events are needed to better understand the new accretion parameterization in models.

Khain et al. (2001) obtained the collision efficiency between graupel particles and cloud droplets as a function of sizes of the individual colliding particle pair using a particle trajectory model. This dataset is used to derive the new accretion parameterization in this study. Khain et al. (2001) adopted flow fields induced by particles that are valid when the Reynolds number is less than 100 (Hamielec and Johnson 1962). The flow fields induced by particles at high Reynolds numbers can be obtained by solving unsteady Navier–Stokes equations numerically. For example, Kubicek and Wang (2012) performed direct numerical simulations (DNSs) to obtain flow fields around a conical graupel. The collision efficiency for various sizes of particles could be obtained by performing a large number of DNSs, although a vast amount of computational resources are needed to accomplish this. This deserves a future investigation.

According to the present study, results from an accretion parameterization that uses the SCE and the collection efficiency of individual particle pairs are different from those from other parameterizations that do not. We suggest that other accretion parameterizations, such as the accretion of cloud water by rain or snow, that generally take into account the simplified SCE can also be improved by adopting the method used in this study.

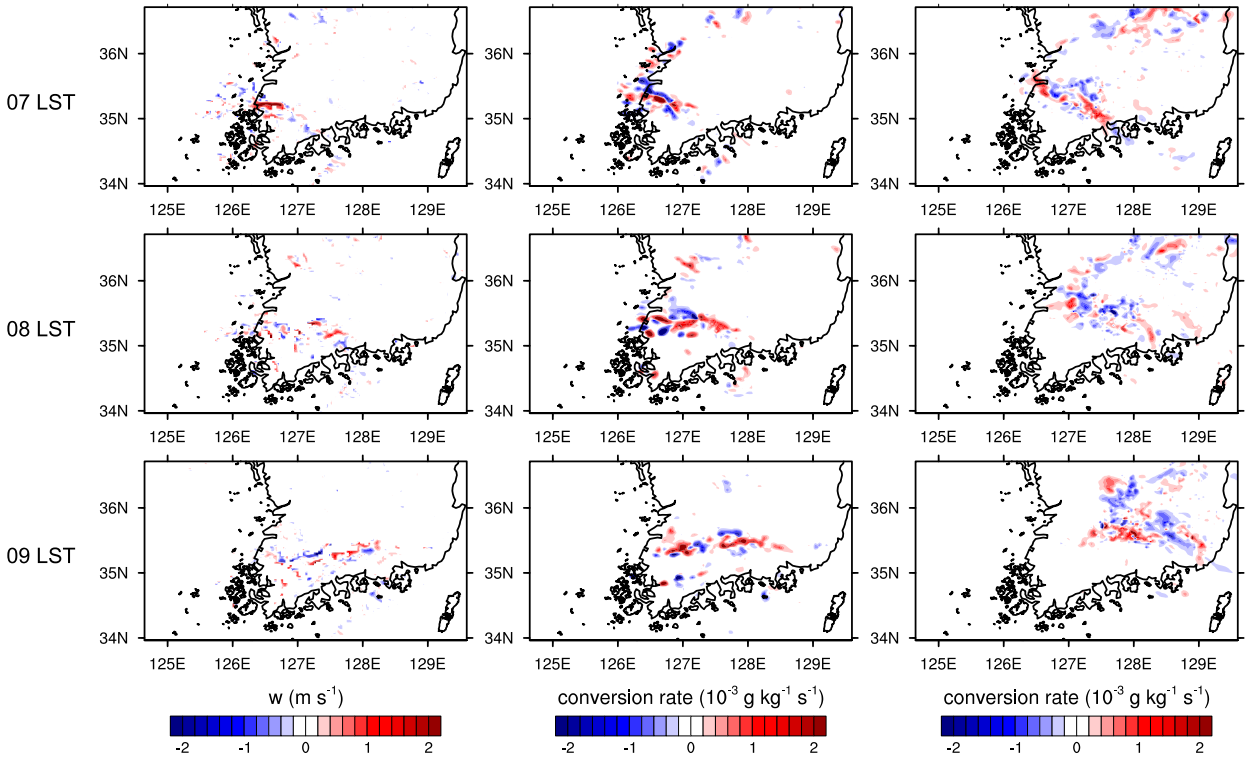

FIG. 15. Differences in (left) the updraft velocity, (center) the melting rate of graupel, and (right) the melting rate of snow at $z = 2$ km between the new parameterization and W72 at $t =$ (top) 0700, (middle) 0800, and (bottom) 0900 LST 15 Mar 2018.

Acknowledgments. The authors are grateful to three anonymous reviewers for providing valuable comments on this work. The authors were supported by the Korea Meteorological Administration Research and Development Program under Grant KMIPA 2015-5190 and by the Basic Science Research Program through the National Research Foundation of Korea (NRF) funded by the Ministry of Science and ICT (2016R1A2B2013549).

REFERENCES

Beard, K. V., 1976: Terminal velocity and shape of cloud and precipitation drops aloft. *J. Atmos. Sci.*, **33**, 851–864, https://doi.org/10.1175/1520-0469(1976)033<0851:TVASOC>2.0.CO;2.

Cober, S. G., and R. List, 1993: Measurements of the heat and mass transfer parameters characterizing conical graupel growth. *J. Atmos. Sci.*, **50**, 1591–1609, https://doi.org/10.1175/1520-0469(1993)050<1591:MOTHAM>2.0.CO;2.

Colarco, P., A. da Silva, M. Chin, and T. Diehl, 2010: Online simulations of global aerosol distributions in the NASA GEOS-4 model and comparisons to satellite and ground-based aerosol optical depth. *J. Geophys. Res.*, **115**, D14207, https://doi.org/10.1029/2009JD012820.

Dudhia, J., 1989: Numerical study of convection observed during the Winter Monsoon Experiment using a mesoscale two-dimensional model. *J. Atmos. Sci.*, **46**, 3077–3107, https://doi.org/10.1175/1520-0469(1989)046<3077:NSOCOD>2.0.CO;2.

Ebert, E. E., 2008: Fuzzy verification of high-resolution gridded forecasts: A review and proposed framework. *Meteor. Appl.*, **15**, 51–64, https://doi.org/10.1002/met.25.

Gaudet, B. J., and J. M. Schmidt, 2005: Assessment of hydrometeor collection rates from exact and approximate equations. Part I: A new approximate scheme. *J. Atmos. Sci.*, **62**, 143–159, https://doi.org/10.1175/JAS-3362.1.

Hamielec, A. E., and A. I. Johnson, 1962: Viscous flow around fluid spheres at intermediate Reynolds numbers. *Can. J. Chem. Eng.*, **40**, 41–45, https://doi.org/10.1002/cjce.5450400202.

Hong, S.-Y., and J.-O. J. Lim, 2006: The WRF single-moment 6-class microphysics scheme (WSM6). *J. Korean Meteor. Soc.*, **42**, 129–151.

——, Y. Noh, and J. Dudhia, 2006: A new vertical diffusion package with an explicit treatment of entrainment processes. *Mon. Wea. Rev.*, **134**, 2318–2341, https://doi.org/10.1175/MWR3199.1.

Kain, J. S., 2004: The Kain–Fritsch convective parameterization: An update. *J. Appl. Meteor.*, **43**, 170–181, https://doi.org/10.1175/1520-0450(2004)043<0170:TKCPAU>2.0.CO;2.

Khain, A. P., and M. Pinsky, 2018: *Physical Processes in Clouds and Cloud Modeling.* Cambridge University Press, 626 pp.

——, ——, M. Shapiro, and A. Pokrovsky, 2001: Collision rate of small graupel and water drops. *J. Atmos. Sci.*, **58**, 2571–2595, https://doi.org/10.1175/1520-0469(2001)058<2571:CROSGA>2.0.CO;2.

——, D. Rosenfeld, A. Pokrovsky, U. Blahak, and A. Ryzhkov, 2011: The role of CCN in precipitation and hail in a mid-latitude storm as seen in simulations using a spectral (bin) microphysics model in a 2D dynamic frame. *Atmos. Res.*, **99**, 129–146, https://doi.org/10.1016/j.atmosres.2010.09.015.

Kovačević, N., and M. Ćurić, 2013: The impact of the hailstone embryos on simulated surface precipitation. *Atmos. Res.*, **132–133**, 154–163, https://doi.org/10.1016/j.atmosres.2013.05.013.

Kubicek, A., and P. K. Wang, 2012: A numerical study of the flow fields around a typical conical graupel falling at various inclination angles. *Atmos. Res.*, **118**, 15–26, https://doi.org/10.1016/j.atmosres.2012.06.001.

Lee, H., and J.-J. Baik, 2017: A physically based autoconversion parameterization. *J. Atmos. Sci.*, **74**, 1599–1616, https://doi.org/10.1175/JAS-D-16-0207.1.

Lin, H., P. K. Wang, and R. E. Schlesinger, 2005: Three-dimensional nonhydrostatic simulations of summer thunderstorms in the humid subtropics versus High Plains. *Atmos. Res.*, **78**, 103–145, https://doi.org/10.1016/j.atmosres.2005.03.005.

Lynn, B. H., A. P. Khain, J. Dudhia, D. Rosenfeld, A. Pokrovsky, and A. Seifert, 2005: Spectral (bin) microphysics coupled with a mesoscale model (MM5). Part I: Model description and first results. *Mon. Wea. Rev.*, **133**, 44–58, https://doi.org/10.1175/MWR-2840.1.

Mansell, E. R., and C. L. Ziegler, 2010: Simulated electrification of a small thunderstorm with two-moment bulk microphysics. *J. Atmos. Sci.*, **67**, 171–194, https://doi.org/10.1175/2009JAS2965.1.

Milbrandt, J. A., and M. K. Yau, 2005: A multimoment bulk microphysics parameterization. Part II: A proposed three-moment closure and scheme description. *J. Atmos. Sci.*, **62**, 3065–3081, https://doi.org/10.1175/JAS3535.1.

Mizuno, H., 1990: Parameterization of the accretion process between different precipitation elements. *J. Meteor. Soc. Japan*, **68**, 395–398, https://doi.org/10.2151/jmsj1965.68.3_395.

Mlawer, E. J., S. J. Taubman, P. D. Brown, M. J. Iacono, and S. A. Clough, 1997: Radiative transfer for inhomogeneous atmospheres: RRTM, a validated correlated-k model for the longwave. *J. Geophys. Res.*, **102**, 16 663–16 682, https://doi.org/10.1029/97JD00237.

Morrison, H., J. A. Curry, and V. I. Khvorostyanov, 2005: A new double-moment microphysics parameterization for application in cloud and climate models. Part I: Description. *J. Atmos. Sci.*, **62**, 1665–1677, https://doi.org/10.1175/JAS3446.1.

Murakami, M., 1990: Numerical modeling of dynamical and microphysical evolution of an isolated convective cloud—The 19 July 1981 CCOPE cloud. *J. Meteor. Soc. Japan*, **68**, 107–128, https://doi.org/10.2151/jmsj1965.68.2_107.

NCEP, 2015: NCEP GDAS/FNL 0.25 degree global tropospheric analyses and forecast grids (updated daily). Computational and Information Systems Laboratory Research Data Archive, accessed 29 May 2018, https://doi.org/10.5065/D65Q4T4Z.

Pruppacher, H. R., and J. D. Klett, 1997: *Microphysics of Clouds and Precipitation.* Kluwer Academic, 954 pp.

Seifert, A., and K. D. Beheng, 2006: A two-moment cloud microphysics parameterization for mixed-phase clouds. Part 1: Model description. *Meteor. Atmos. Phys.*, **92**, 45–66, https://doi.org/10.1007/s00703-005-0112-4.

Skamarock, W. C., and Coauthors, 2008: A description of the Advanced Research WRF version 3. NCAR Tech. Note TN-475+STR, 113 pp., https://doi.org/10.5065/D68S4MVH.

Stevens, B., G. Feingold, W. R. Cotton, and R. L. Walko, 1996: Elements of the microphysical structure of numerically simulated nonprecipitating stratocumulus. *J. Atmos. Sci.*, **53**, 980–1006, https://doi.org/10.1175/1520-0469(1996)053<0980:EOTMSO>2.0.CO;2.

Tewari, M., and Coauthors, 2004: Implementation and verification of the unified Noah land surface model in the WRF Model. *20th Conf. on Weather Analysis and Forecasting/16th Conf. on Numerical Weather Prediction*, Seattle, WA, Amer. Meteor. Soc., 14.2a, https://ams.confex.com/ams/84Annual/techprogram/paper_69061.htm.

Thompson, G., and T. Eidhammer, 2014: A study of aerosol impacts on clouds and precipitation development in a large winter cyclone. *J. Atmos. Sci.*, **71**, 3636–3658, https://doi.org/10.1175/JAS-D-13-0305.1.

——, P. R. Field, R. M. Rasmussen, and W. D. Hall, 2008: Explicit forecasts of winter precipitation using an improved bulk microphysics scheme. Part II: Implementation of a new snow parameterization. *Mon. Wea. Rev.*, **136**, 5095–5115, https://doi.org/10.1175/2008MWR2387.1.

Verlinde, J., P. J. Flatau, and W. R. Cotton, 1990: Analytical solutions to the collection growth equation: Comparison with approximate methods and applications to cloud microphysics parameterization schemes. *J. Atmos. Sci.*, **47**, 2871–2880, https://doi.org/10.1175/1520-0469(1990)047<2871:ASTTCG>2.0.CO;2.

Wang, J., and K. P. Georgakakos, 2005: Effects of cold microphysical processes on the surface precipitation variability of nonsquall tropical oceanic convection. *J. Geophys. Res.*, **110**, D22203, https://doi.org/10.1029/2005JD005787.

Weisman, M. L., and J. B. Klemp, 1982: The dependence of numerically simulated convective storms on vertical wind shear and buoyancy. *Mon. Wea. Rev.*, **110**, 504–520, https://doi.org/10.1175/1520-0493(1982)110<0504:TDONSC>2.0.CO;2.

Wisner, C., H. D. Orville, and C. Myers, 1972: A numerical model of a hail-bearing cloud. *J. Atmos. Sci.*, **29**, 1160–1181, https://doi.org/10.1175/1520-0469(1972)029<1160:ANMOAH>2.0.CO;2.

Zhang, D.-L., and R. A. Anthes, 1982: A high-resolution model of the planetary boundary layer—Sensitivity tests and comparisons with SESAME-79 data. *J. Appl. Meteor.*, **21**, 1594–1609, https://doi.org/10.1175/1520-0450(1982)021<1594:AHRMOT>2.0.CO;2.